PHILOSOPHICAL MAGAZINE, 2003, VOL. 83, NO. 12, 1451–1461

Determination of the B1–B2 transition path in RbCl by Möbius pair potentials

SHUO ZHANG†‡‖ and NAN-XIAN CHEN†‡§

† Department of Physics, Tsinghua University, 100084 Beijing, PR China
‡ National Key Laboratory for Materials Simulation and Design, 100083 Beijing, PR China
§ Institute for Applied Physics, University of Science and Technology Beijing, 100083, Beijing, PR China

[*Received 28 July 2002 and accepted in revised form 12 December 2002*]

ABSTRACT

Using Chen–Möbius lattice inversion, we derive the interionic pair potentials from pseudopotential total-energy curves of the RbCl polymorph. Based on the potentials, the B1–B2 transition pathways have been analysed by calculating the activation energy and saddle point at transition pressure. The intermediate structures along the transition path were obtained within the different symmetric restrictions. By comparing the four pathways under the different restricted conditions, the intermediate structures with space groups *Cmcm* and $P2_1/m$ were predicted to explain the B1–B2 phase transition in RbCl.

§ 1. INTRODUCTION

The high-pressure-induced B1–B2 phase transition in RbCl has been reported at 0.5 GPa by Onodera *et al.* (1992). During their neutron diffraction study, a displacive mechanism with several martensitic-like properties was proposed to explain the mixture of B1 and B2 phases at the transition. This mechanism, to some extent, is consistent with the Buerger mechanism (Wert 1984, Pendás *et al.* 1994), which is often used to explain the B1–B2 phase transition. Although the crystal orientation relations of the B1–B2 transition in RbCl has been interpreted by this mechanism, some neutron and X-ray diffraction studies (Kusaba *et al.* 1995, Hull and Keen 1999) suggested there was an intermediate phase with the KOH-type structure existing in the transition. In order to clarify this confusion, the X-ray absorption fine-structure data on powdered RbCl were obtained by Kelly *et al.* (1998) to determine the structure of RbCl at transition. Their results indicated that there was no evidence for an intermediate phase. It seems that the results of Onodera *et al.* and Kelly *et al.* (1998) all supported the fact that the B1 and B2 phases were connected by the coexistence of both phases. However, since the B1–B2 phase transition is a complicated process, it is possible that there are several different intermediate phases besides the KOH-type structure. Therefore, the fitting employed by Kelly *et al.* which was based only on the KOH-type structure might miss the

‖ Author for correspondence. Email: zhangshuo@mails.tsinghua.edu.cn.

Philosophical Magazine ISSN 1478–6435 print/ISSN 1478–6443 online © 2003 Taylor & Francis Ltd
http://www.tandf.co.uk/journals
DOI: 10.1080/1478643031000080717

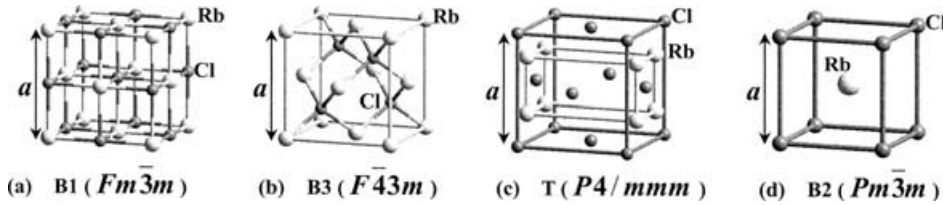

Figure 1. Structures used for the pseudopotential total-energy calculations.

possibility of other intermediate phases. Therefore the goal of this work is to find the possible intermediate structure along the B1–B2 transition path in RbCl.

In order to determine the intermediate phases at transition in RbCl, the appropriate interionic potentials are needed to analyse the Gibbs energy surface from the B1 to the B2 phase. However, the previous interionic potentials (Sangster and Dixon 1976, Catlow *et al*. 1977, Jacobs and Vernon 1998) for RbCl were almost obtained only from the properties of the B1 phase. That makes it very difficult to judge whether this kind of potential can correctly describe the Gibbs free energy at transition pressure. Therefore, based on Chen–Möbius lattice inversion (Chen *et al*. 1997, 1998), a new kind of interionic pair potential is derived from the pseudopotential total-energy curves of RbCl polymorph in this paper. According to this scheme, not only the B1 phase but also B2, B3 and T (with space group $P4/mmm$) structures are involved to obtain the pair potentials (figure 1). Also, since the total-energy calculations are performed for lattice constants $a = 5.5$ to 16.0 Å, some non-equilibrium states are also included so that the interionic pair potentials may be valid over a wide range of interionic spacings. Thus it is possible that the B1–B2 transition path could be correctly described by the Möbius pair potentials.

With the Möbius pair potentials, the B1–B2 transition path can be determined as the minimum-energy trace on the Gibbs energy hypersurface. According to the Buerger and the WTM (Watanabo, Tokonami and Motimoto) mechanisms (Sims *et al*. 1998), the transition is considered to take place along the $R\bar{3}m$ and $Pmm2$ pathways respectively. However, both the Buerger and the WTM mechanisms cannot predict the intermediate phase with KOH-type structure (Kusaka *et al*. 1995), which has the space group $P2_1/m$. The reason is that the transition path was determined with more symmetric restrictions. Therefore, in this paper, the transition path is determined with fewer symmetric restrictions in the eight-ion standard cell. The details are described in the following text.

§2. Derivation of Möbius pair potentials

According to lattice inversion (Chen *et al*. 1997, 1998), in order to extract three kinds of pair potential, ϕ_{+-} , ϕ_{--} and ϕ_{++} , we calculated the pseudopotential total-energy curves of RbCl in the B1, B2, B3 and T structures with lattice constants a from 4.0 to 16.0 Å. These calculations were performed via the CASTEP (1998) software package (Segall *et al*. 2002). In this paper, the ultrasoft pseudopotentials were used and the exchange–correlation energy was taken into account by the generated gradient approximation method. The k-mesh points over Brillouin zone were generated with parameters $4 \times 4 \times 4$ for the largest reciprocal space and $1 \times 1 \times 1$ for the smallest reciprocal space by the Monkhorst–Pack (1976) scheme corresponding to the lattice constant. The energy tolerance for self-consistent field convergence

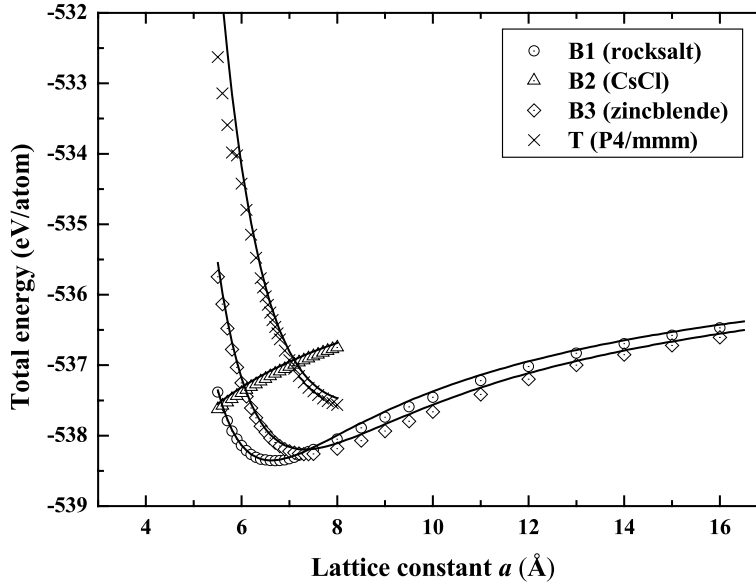

Figure 2. Total energy versus lattice constant a of the RbCl polymorph (⊙), (△), (◇), (×), from the CASTEP calculations; (——), calculated on the basis of pair potential.

is 2×10^{-6} eV atom^{-1}. The kinetic energy cut-off for the plane-wave basis set is 260 eV. The total energy as a function of lattice constant a is shown in figure 2.

The interionic pair potential is usually decomposed into Coulombic and non-Coulombic terms. For the Coulombic part, since the electrostatic potential is slowly convergent, the effective charges are determined by fitting to the total-energy difference between B1 and B3 KCl for lattice constants a from 10.0 to 16.0 Å. With the Madelung constants in B1 and B3 structures (Kittel 1996), the effective charge is $0.991e$. For the non-Coulombic contribution, with the identical lattice constant a, the difference between B1 and B3 structures is only about the Rb^+–Cl^- distance. Then the total-energy difference $E_{B1} - E_{B3}$ between B1 and B3 should only depend on the Rb^+–Cl^- pair potential and can be written as

$$E_{B1} - E_{B3} = \tfrac{1}{2}\left(\sum_{B1} \phi_{+-}(r_{ij}) - \sum_{B3} \phi_{+-}(r_{ij})\right), \tag{1}$$

where ϕ_{+-} is the cation–anion pair potential and r_{ij} is the separation between ions at lattice sites i and j ($i \neq j$). Then ϕ_{+-} can be solved from equation (1) by Chen–Möbius lattice inversion (Chen *et al.* 1997, 1998).

For the anion–anion potential, since the B1 and T structures have the same Rb^+ sublattice for the lattice constant a, the total-energy difference $E_{B1} - E_T$ between B1 and T should be independent of the cation–cation spacing and can be expressed as

$$E_{B1} - E_T = \tfrac{1}{2}\left(\sum_{B1} \phi_{+-}(r_{ij}) + \sum_{B1} \phi_{--}(r_{ij}) - \sum_{T} \phi_{+-}(r_{ij}) - \sum_{T} \phi_{--}(r_{ij})\right). \tag{2}$$

With the same lattice inversion techniques and the above pair potential ϕ_{+-}, the anion–anion pair potential ϕ_{--} can also be obtained from equation (2).

Table 1. Interionic pair potential parameters obtained in this work. The symbols + and − represent cation and anion, respectively. The cut-off distance for short-range potential is 12.0 Å. The function forms are described as follows:

$$\phi(r_{ij}) = \phi^{\mathrm{SR}}(r_{ij}) + \frac{q_i q_j}{4\pi\varepsilon_0 r_{ij}}$$

The Morse form is:

$$\phi^{\mathrm{SR}}(r_{ij}) = D\left\{ \exp\left[-\gamma\left(\frac{r_{ij}}{R} - 1\right)\right] - 2\exp\left[-\frac{\gamma}{2}\left(\frac{r_{ij}}{R} - 1\right)\right]\right\}.$$

The repulsive-exponential (Rep.-Exp.) form

$$\phi^{\mathrm{SR}}(r_{ij}) = D\exp\left[-\gamma\left(\frac{r_{ij}}{R} - 1\right)\right].$$

Ion pair	$\phi^{\mathrm{SR}}(r_{ij})$	D (eV)	R (Å)	γ
++	Rep.-Exp.	0.0572	2.6860	8.7701
+−	Rep.-Exp.	0.5099	2.9085	8.2691
−−	Morse	0.0870	3.9386	7.8972

Since the cation–anion and anion–anion interactions can be calculated for four structures, the cation–cation pair potential ϕ_{++} can also be derived from the total-energy difference between B1 and B2 RbCl crystals by the lattice inversion method. Based on the final potential curves, suitable function forms are selected to express the interionic pair potentials. The final potential parameters are listed in table 1.

§ 3. Static properties of B1 and B2 RbCl

In order to test the quality of the potentials, the Möbius pair potentials were firstly used to calculate the total energy curves of RbCl in the above four structures (see figure 2). The result indicates that the interionic pair potentials have been correctly obtained by Chen–Möbius inversion. With these pair potentials, we calculated the static properties of B1 and B2 RbCl, for example the equilibrium lattice constant a_0, bulk modulus B_0, lattice energy E_{latt} and volume V_0 at zero temperature and pressure. The results in table 2 indicate that the present calculations

Table 2. Calculated static properties of B1 and B2 RbCl at zero pressure.

Structure	Reference	Lattice constant a_0 (Å)	Bulk modulus B_0 (GPa)	Lattice energy E_{latt} (kcal mol^{-1})	Volume at 0 Pa V_0 (Å^3 pair^{-1})
B1	This work	6.616	16.59	160.15	72.40
	Recio *et al.* (1993)	6.782	15.3	159.5	77.99
	Cohen *et al.* (1975)	6.52	18.5	165.0	69.29
	Experiment (Sodeshmukh *et al.* 2001)	6.5898	15.6	159.3	71.541
B2	This work	3.978	19.94	158.01	62.96
	Recio *et al.* (1993)	3.994	19.3	159.2	63.71
	Cohen *et al.* (1975)	3.90	—	162.7	59.32
	Experiment (Recio *et al.* (1993))	3.934	18.2	—	60.9

are in good agreement with the experimental data (Sodeshmukh *et al.* 2001) and previous calculations (Cohen and Gordon 1975, Recio *et al.* 1993).

Besides these static properties, the 0 K Gibbs free energies $G_0 = E + pV$ of B1 and B2 RbCl can also be calculated at different pressures. Then the Gibbs energy difference $\Delta G_0 = G_0(\mathrm{B1}) - G_0(\mathrm{B2})$ per ionic pair can be obtained by minimization of G_0 versus the cubic cell parameters for each phase at different pressures. This gives the result $\Delta G_0 = -1.969 + 1.145p$, with p in gigapascals and G_0 in kilocalories per mole. The equilibrium condition $\Delta G_0 = 0$ yields $p_{\mathrm{tr}} = 1.72$ GPa as the transition pressure. Although this value is very close to $p_{\mathrm{tr}} = 1.71$ GPa obtained by Cohen and Gordon (1975), it is higher than the experimental value $p_{\mathrm{tr}} = 0.5$ GPa (Onodera *et al.* 1992). The reason may be that the present pair potentials overestimate the lattice energy of the B1 phase (see table 2), therefore leading to a higher transition pressure. However, to some extent, this calculated value could be comparable with the experimental data. The calculated static properties are consistent with the experimental data (Sodeshmukh *et al.* 2001) and previous calculations (Cohen and Gordon 1975, Recio *et al.* 1993). Thus, it is still believable that the present pair potentials, from the total-energy curves of the RbCl polymorph, could be used to explore the B1–B2 transition path at high pressures.

§4. Determination of the transition path from the B1 to the B2 phase

In this work, the eight-ion standard cell was used to determine the B1–B2 transition path for RbCl. The reason is that both the two-ion rhombohedral and the four-ion orthorhombic cells cannot simultaneously exhibit the transition characters of the Buerger and the WTM mechanisms respectively. Therefore it is hoped that the eight-ion cubic cell can totally describe the transition characters of the Buergers and the WTM mechanisms.

Based on the Möbius pair potentials, the final configuration of the B2 phase was obtained by energy minimization from the initial B1 structure at 10 GPa, as shown in figure 3. According to this final configuration of the B2 phase, four transition pathways could be determined at the transition pressure p_{tr} as follows.

The first path is determined as (a, a, a, a, a, a) with $R\bar{3}m$ symmetry (Pendás *et al.* 1994, Sims *et al.* 1998) and is called path I. Along this path, every intermediate structure was obtained by optimizing the cell length $a = b = c$ for each fixed cell

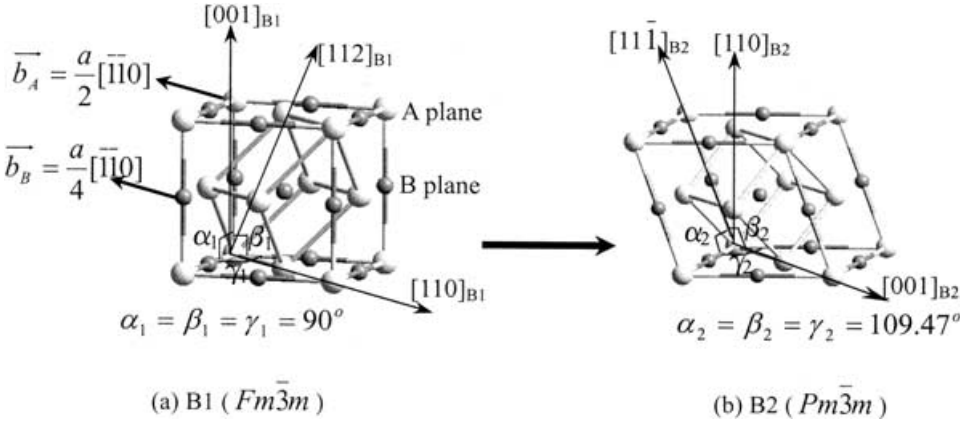

Figure 3. The initial and final configurations in the B1–B2 phase transition of RbCl.

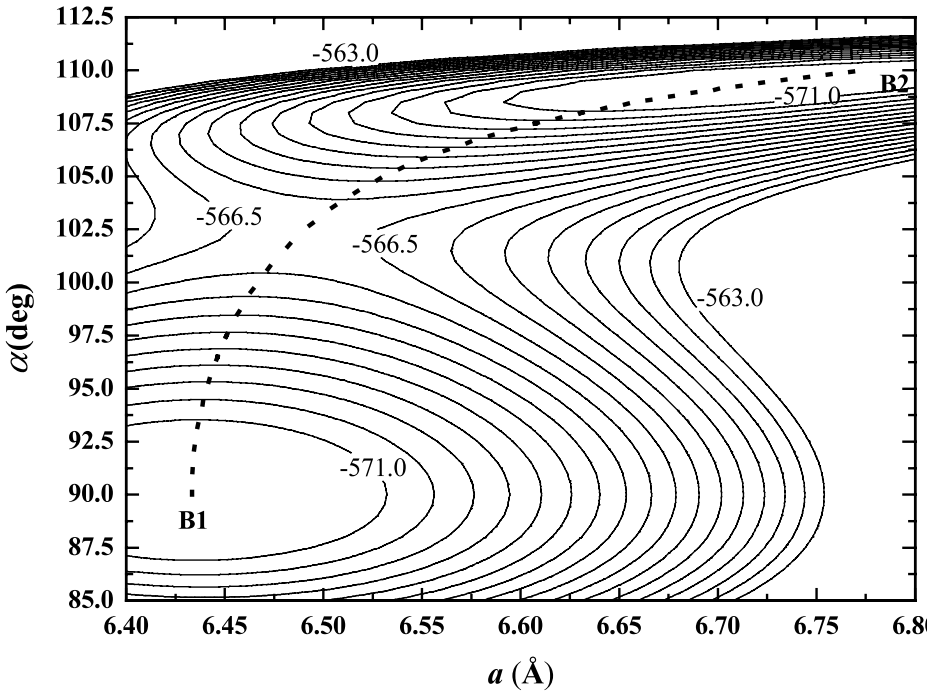

Figure 4. Contour plot of the $R\bar{3}m$ 0 K Gibbs energy minimum (in kilocalories per mole) as a function of the cell parameters a and α.

angle $\alpha = \beta = \gamma$ within the restriction of $R\bar{3}m$ symmetry. When the cell angles simultaneously increase from 90° to 109.47°, the B1 RbCl transforms into the high-pressure-induced B2 phase. Then the path at transition pressure can be described by the coupling of the cell parameters a and α, as shown by the dotted curve in figure 4. From figure 4 it is also obvious that the B1–B2 transition at p_{tr} is the activation process with an energy barrier between the initial and final phases.

Since the $R\bar{3}m$ symmetry is always held to determine the intermediate phase from B1 to B2, there is no other intermediate structure found along path I. Therefore, it is difficult to explain whether or not there is the existence of an intermediate phase with KOH-type structure like the B1–B2 transition in AgCl (Kusaba *et al.* 1995). In order to find other intermediate structures, the transition path should be determined with fewer symmetry restrictions. First, we define path II where the restriction is that the three cell angles are all equal ($\alpha = \beta = \gamma$). Then, from $\alpha = \beta = \gamma = 90°$ to $\alpha = \beta = \gamma = 109.47°$, every intermediate structure is obtained by optimizing the cell lengths a, b and c and the inner atomic positions to the minimum energy for each group of cell angles ($\alpha = \beta = \gamma$). Secondly, the restriction is reduced to $\beta = \gamma$; then path III is composed of a series of intermediate states, which have the minimum Gibbs energy by adjusting the cell parameters a, b, c and α and inner atomic co-ordinations for each $\beta = \gamma$. Finally, each intermediate configuration of path IV is decided by freely adjusting the cell parameters a, b, c, α and β and inner atomic positions to make the energy minimum for every cell angle γ from 90° to 109.47°.

In order to compare the four transition pathways from the B1 phase ($a_1 = b_1 = c_1$, $\alpha_1 = \beta_1 = \gamma_1 = 90°$) to the B2 phase ($a_2 = b_2 = c_2$, $\alpha_2 = \beta_2 = \gamma_2 = 109.47°$), the volume V_0 per RbCl pair is taken as the reaction factor

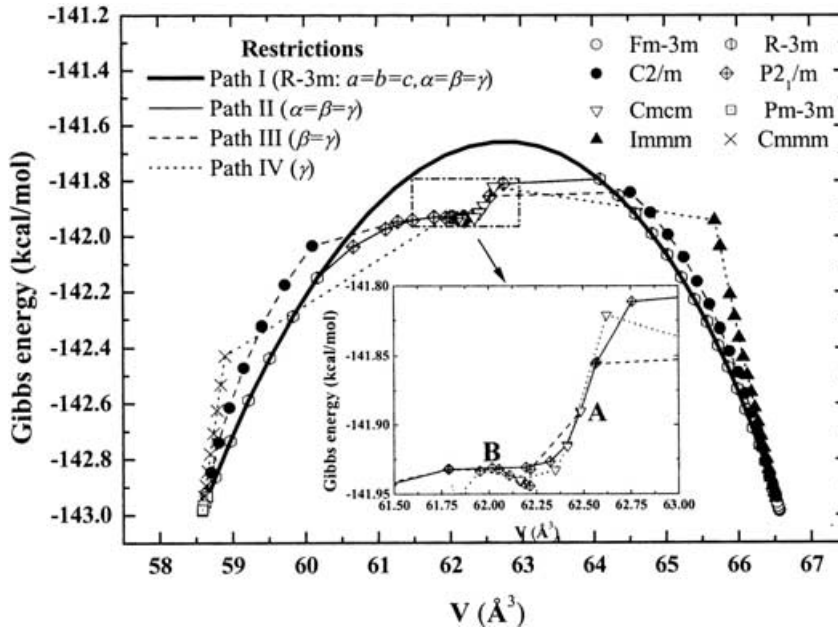

Figure 5. Calculated minimum-energy pathways of paths I, II, III and IV as functions of the volume per ionic pair.

to characterize the phase transition. Then the activation energy barriers of four transition pathways are shown in figure 5, and the corresponding structural parameters of intermediate phases are described in figures 4 and 6, respectively.

§ 5. Results and Discussions

From figure 5 it is clear that the symmetry restriction plays an important role in the determination of the B1–B2 transition path at p_{tr}. Along path I, the intermediate phases have the space group $R\bar{3}m$, which is the highest common subgroup between $Fm\bar{3}m$ (B1) and $Pm\bar{3}m$ (B2) (Kusaka *et al.* 1995). Therefore the atomic positions at the limit structures must correspond to particular selections of the free coordinates in the path I cell. In this way, the unrestricted cell parameters of path I are a and α. The dotted curve in figure 4 indicates the lowest-energy path in the $R\bar{3}m$ phase space. As a result of the decrease in symmetry restriction, the transition pathways include several parts with different space groups. Path II is $Fm\bar{3}m \rightarrow R\bar{3}m \rightarrow P2_1/m \rightarrow Cmcm - P2_1/m \rightarrow R\bar{3}m \rightarrow Pm\bar{3}m$. This indicates the parts near the initial B1 phase and the final B2 phase is also present along the $R\bar{3}m$ path, but the parts around the saddle point change greatly into the lower symmetries. To our surprise, the intermediate states around the saddle point have space groups similar to those of the AgCl intermediate structures KOH and TlI (Kusaba *et al.* 1995). When the restriction is reduced from $\alpha = \beta = \gamma$ to $\beta = \gamma$, along path III, the intermediate structures with the space group $C2/m$ are the dominant parts near the initial and final phases at transition, and the part around the saddle point is also composed of $P2_1/m$ and $Cmcm$ structures. When fixing the angle γ is the only restriction, path IV includes the $Immm$ part near the B1 state and the $Cmmm$ part near the B2 configuration, but the saddle part is also formed by $P2_1/m$ and $Cmcm$ structures.

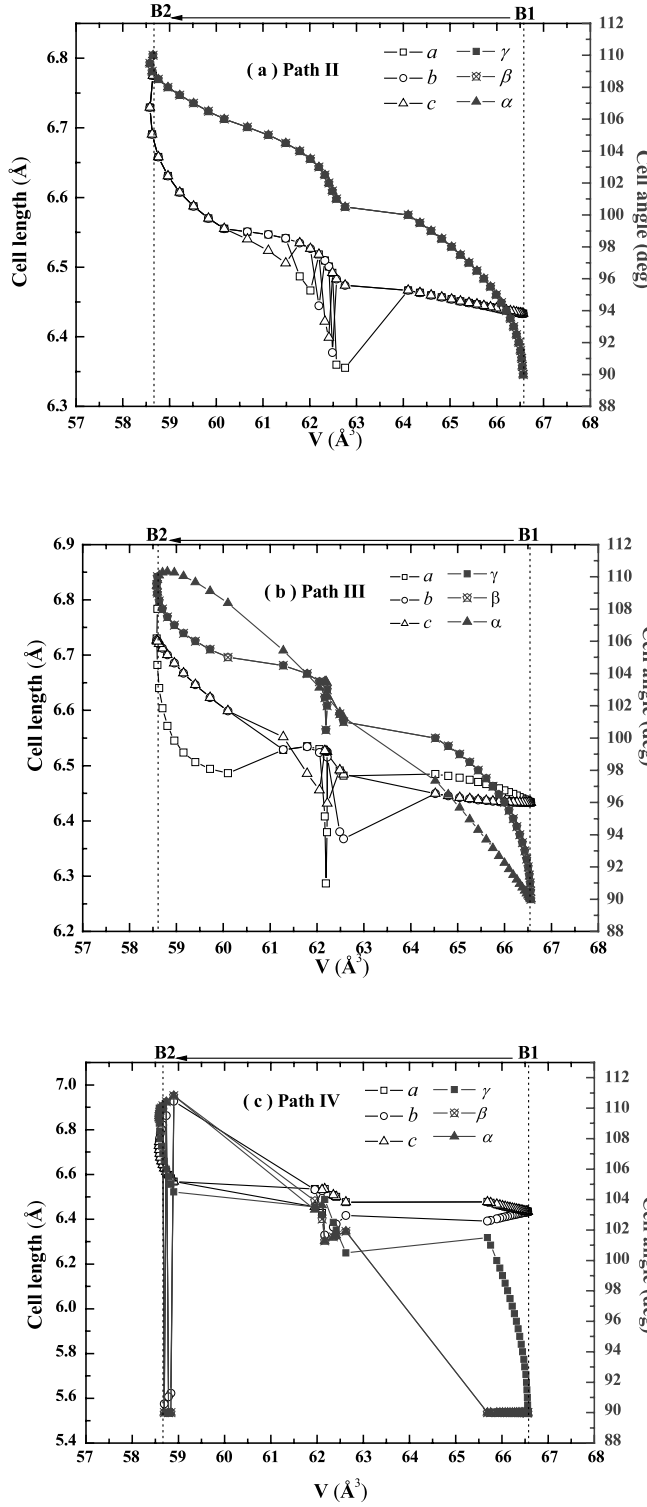

Figure 6. The variations in cell parameters along paths II, III and IV.

Although the saddle parts of paths II, III and IV are not exactly identical, it is clear that their differences are very tiny so that the $P2_1/m$ and *Cmcm* structures are predicted as the important intermediate phases from the B1 phase to the B2 phase for RbCl.

In addition, paths I, II, III and IV all indicate that the B1–B2 phase transition is an activation process at p_{tr}. From figure 5 we can see that their activation energies are $1.325\,\mathrm{kcal\,mol^{-1}}$, $1.190\,\mathrm{kcal\,mol^{-1}}$, $1.142\,\mathrm{kcal\,mol^{-1}}$ and $1.164\,\mathrm{kcal\,mol^{-1}}$ for paths I, II, III and IV respectively. It is obvious that the transition pathways with fewer symmetric restrictions have lower activation-energy barriers. However, the difference in their energy barriers is not more than $0.183\,\mathrm{kcal\,mol^{-1}}$; so the barriers of paths II, III and IV are still comparable with that of path I. This may be one important reason why the $R\bar{3}m$ path of Buerger mechanism can basically describe the B1–B2 phase transition for alkali halides.

Also, it can be seen from figure 5 that the restriction difference from path II to path IV has almost no influence on their activation energies. However, their transition pathways in figures 5 and 6 are obviously different, especially for the initial and final stages. With the decrease in symmetric restrictions, drastic changes in volume take place from the B1 to the B2 phase, especially for paths III and IV. This leads to an obvious reduction in translational symmetry for intermediate structures. This also indicates that the defect may be produced with the strong variations in cell parameters in figure 6. To some degree, this may be regarded as the fact that the phase transition is not an extremely cooperative and concerted process, and the defects play a very important role in the kinetics of the transition. This is consistent with the experimental observations (Zaretsky 1998).

Since $P2_1/m$ and *Cmcm* structures exist in our calculations, and Kelly *et al.* (1998) found no evidence for an intermediate phase, it is desirable to know the relationship between the B1–B2 coexistence and the intermediate structures. Therefore the *Cmcm* structure with a volume of 62.5 Å and the $P2_1/m$ cell with a volume of 62.0 $\mathrm{Å}^3$ were chosen to be studied further; the reason is that these two structures are the common points for paths II, III and IV, as shown by points A and B in figure 5. From the B1 to the B2 phase, the lattices projected along the [001] direction are shown in figure 7. In order to show the structural variation, the corresponding radial distribution function (RDF) is also shown in figure 7. For the $Fm\bar{3}m$, $P2_1/m$, *Cmcm* and $Pm\bar{3}m$ phases, their angles θ between the [100] and [011] directions are 90°, 105.2°, 109.3° and 125.3° respectively. Since the angle values for intermediate structures are very close to those of the KOH and TlI intermediate phases of AgCl (Kusaba *et al.* 1995), and their space groups are exactly identical, therefore we think that the present intermediate phases have similar structures to those of KOH and TlI. The difference between AgCl and RbCl is the transition sequence, which was found to be $Fm\bar{3}m \rightarrow P2_1/m \rightarrow Cmcm \rightarrow Pm\bar{3}m$ for AgCl (Kusaba *et al.* 1995), and the present sequence is $Fm\bar{3}m \rightarrow Cmcm \rightarrow P2_1/m \rightarrow Pm\bar{3}m$. This indicates that the transition in RbCl may not be a process in which the cell angle is monotonical increasing from 90° to 125.3°. Irrespective of how the angle changes in the B1–B2 transition, it is clear that the *Cmcm* phase has the characters of both the B1 and the B2 phase, as shown in figure 7. It may be proposed that the *Cmcm* structure is formed by alternately stacking B1 and B2 units along the [010] directions. As for the $P2_1/m$ intermediate phase, its basic unit is obviously different from those of the B1 and B2 phases. From this viewpoint, it may be concluded that the *Cmcm* structure is superior to the $P2_1/m$ state for

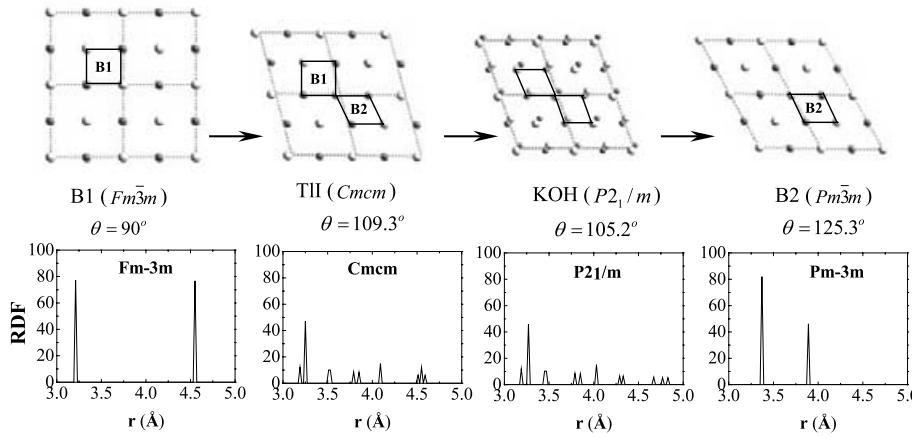

Figure 7. Crystal structures of the $Fm\bar{3}m$, $Cmcm$, $P2_1/m$ and $Pm\bar{3}m$ phases projected on to the (001) plane. The characters of the NaCl (B1), TlI, KOH and CsCl (B2) structures respectively are shown.

characterizing the coexistence of B1 and B2 phases, despite their similar RDFs in figure 7. This may be the reason why Kelly *et al.* (1998), who used the $P2_1/m$ structure, obtained unsatisfactory results because they missed the *Cmcm* phase. From these results we concluded that the mixture of phases should be characterized by the *Cmcm* structure.

Above all, we can show a simple mechanism for the B1–B2 transition under high pressures for RbCl. From the B1 to the B2 phase as shown in figure 3 and 7, the [001] direction of the B1 structure changes into the $[11\bar{1}]$ direction of the B2 phase, the [112] direction of the B1 phase shortens and converts to the [110] direction of the B2 phase, and the [110] direction of the B1 phae transforms into the [001] direction of the B2 phase. If viewing along the [001] direction of the B1 phase, we can also see that the [001] direction of the B1 structure is parallel to the [110] direction of the B2 structure. These crystal orientation relationships are consistent with the observations from X-ray and neutron diffractions (Onodera *et al.* 1992). Also from the initial and final configurations it can be seen that the rhombohedral unit is compressed along the [111] direction into a cubic unit for accomplishing the B1–B2 transition, this is the character of the Buerger mechanism (West 1984, Pendás *et al.* 1994). As for the adjacent (001) planes of the B1 structure, the A plane glides with the Burgers vector $\mathbf{b}_A = (a/2)[1\bar{1}0]$, and the B plane glides with Burgers vector $\mathbf{b}_B = (a/4)[1\bar{1}0]$; this results in the relative translation with Burgers vector $\mathbf{\Delta} = (a/4)[1\bar{1}0]$. This character can be described by WTM mechanism (Sims *et al.* 1998). Therefore it is possible that both the characters of both the Buerger and the WTM mechanisms can be described by the eight-ion standard cell. During the B1–B2 transition, the transition path includes several parts with different space groups belonging to the common subgroups of $Fm\bar{3}m$ and $Pm\bar{3}m$, in which the *Cmcm* and $P2_1/m$ structures are predicted as the most valuable intermediate phases.

§6. Conclusions

Based on the Chen–Möbius lattice inversion, the interionic pair potentials have been obtained from the pseudopotential total-energy curves of RbCl in the B1, B2,

B3 and $P4/mmm$ structures. With these potentials, the B1–B2 transition pathways are determined and the influence of symmetric restrictions has also been discussed in detail. The pathways with different symmetric restrictions indicate that the activation energy and saddle point are almost unaffected by the various translation symmetries, and the *Cmcm* and $P2_1/m$ structures are predicted as the intermediate phases from the B1 to the B2 phases. In particular, the *Cmcm* structure can be used to characterize the mixture of B1 and B2 phases. This may explain whether or not there is intermediate phase from the B1 to the B2 phase in RbCl. The overall results reveal that the present Möbius pair potentials are valid over a wide range of interionic separations and can provide important information for the B1–B2 transition path in RbCl.

Acknowledgements

This work was supported in part by the National Science Foundation of China, and in part by the National Advanced Materials Committee of China. Special thanks should be given to the support from the 973 Project in China (grant G2000067101) and the National Nature Science Foundation of China (grant 10274035).

References

CASTEP Molecular Simulation Software, San Diego, 1998.

Catlow C. R. A., Diller K. M., and Norgett, M. J., 1977, *J. Phys.* C, **10**, 1395.

Chen, N.-X., Chen, Z.-D., and Wei, Y.-C., 1997, *Phys. Rev.* E, **55**, R5.

Chen, N.-X., Ge, X.-J., Zhang, W.-Q., and Zhu, F.-W., 1998, *Phys. Rev.* B, **57**, 14 203.

Cohen, A. J., and Gordon, R. G., 1975, *Phys. Rev.* B, **12**, 3228.

Hull, S., and Keen, D. A., 1999, *Phys. Rev.* B, **59**, 750.

Jacobs, P. W. M., and Vernon, M. L., 1998, *Can. J. Chem.,* **76**, 1540.

Kelly, S., Ingalls, R., Wang, F., Ravel, B., and Haskel, D., 1998, *Phys. Rev.* B, **57**, 7543.

Kittel, C., 1996, *Introduction to Solid State Physics,* seventh edition (New York: Wiley), pp. 66–72.

Kusaba, K., Syono, Y., Kikegawa, T, and Shimomura, O., 1995, *J. Phys. Chem. Solids,* **56**, 751.

Monkhorts, H. J., and Pack, J. D., 1976, *Phys. Rev.* B, **13**, 5188.

Onodera, A., Kawano, S., Nakai, Y., and Achiwa, N., 1992, *Physica* B, **180–181**, 279.

Pendás, A. M., Luaña, V., Recio, J. M., Flórez, M., Francisco, E., Blanco, M. A., and Kantorovich, L. N., 1994, *Phys. Rev.* B, **49**, 3066.

Recio, J. M., Pendás, A. M., Francisco, E., Flórez, M., and Luaña, V., 1993, *Phys. Rev.* B, **48**, 5891.

Sangster, M. J. L., and Dixon, M., 1976, *Adv. Phys.,* **25**, 247.

Segall, M. D., Lindan, P. J., Prober, M. J., Pickard, C. J., Hasnip, P. J., Clark, S. J., and Payne, M. C., 2002, *J. Phys. condens. Matter,* **14**, 2717.

Sims, C. E., Barrera, G. D., and Allan, N. L., 1998, *Phys. Rev.* B, **57**, 11 164.

Sirdeshmukh, D. B., Sirdeshmkh, L., and Subhadra, K. G., 2001, *Alkali Halides—A Handbook of Physics Properties* (Berlin; Springer), pp. 6–50.

West, A. R., 1984, *Solid State Chemistry and Its Applications* (New York: Wiley).

Zaretsky, E., 1998, *J. Phys. Chem. Solids,* **59**, 253.